

# How can the *James Webb Space Telescope* measure First Light, Reionization, and Galaxy Assembly?

Rogier Windhorst, Rolf Jansen, Seth Cohen, Matt Mechtley (ASU), Haojing Yan (OCIW) & Chris Conselice (Nottingham)

## Abstract

In this poster, we briefly review the capabilities of the 6.5 m James Webb Space Telescope (JWST) — slated for launch to a halo L2 orbit in 2013 — including the considerations to make this an optimized infrared telescope that can deploy automatically in space.

The main science themes of JWST are to measure First Light, Reionization, Galaxy Assembly, as well as the process of Star-formation and the origin of Planetary Systems. Here, we summarize how JWST will go about measuring First Light, Reionization, and Galaxy Assembly, building on lessons learned from the Hubble Space Telescope — the Hubble UltraDeep Field (HUDF) in particular.

We show what relatively nearby galaxies, observed in their rest-frame UV–optical light, will likely look like to JWST at very high redshifts, and discuss quantitative methods to determine the structural parameters of faint galaxies in deep JWST images as a function of cosmic epoch. We also discuss to what extent JWST’s short wavelength performance — which needed to be relaxed in the 2005 definition of the telescope — may affect JWST’s ability to accurately determine faint galaxy parameters.

We also discuss if ultradeep JWST images will run into the natural confusion limit, and what new generations of algorithms may be needed to automatically detect objects in very crowded, ultradeep JWST fields.

For an interactive web-tool that lets the user pan and zoom through the HUDF data-base from redshifts  $z=0$  to  $z=6$  and visualize what JWST will add at  $AB=29.5\text{--}32.0$  mag (redshifts  $z\sim 7\text{--}20$ ), we refer to poster 218.12 by L. Will et al.

This work was funded by NASA JWST Interdisciplinary Scientist grant NACS-12460 from GSFC, and grant HST/ED14-975 from STScI, which is operated by AURA for NASA under contract NAS 5-26555.

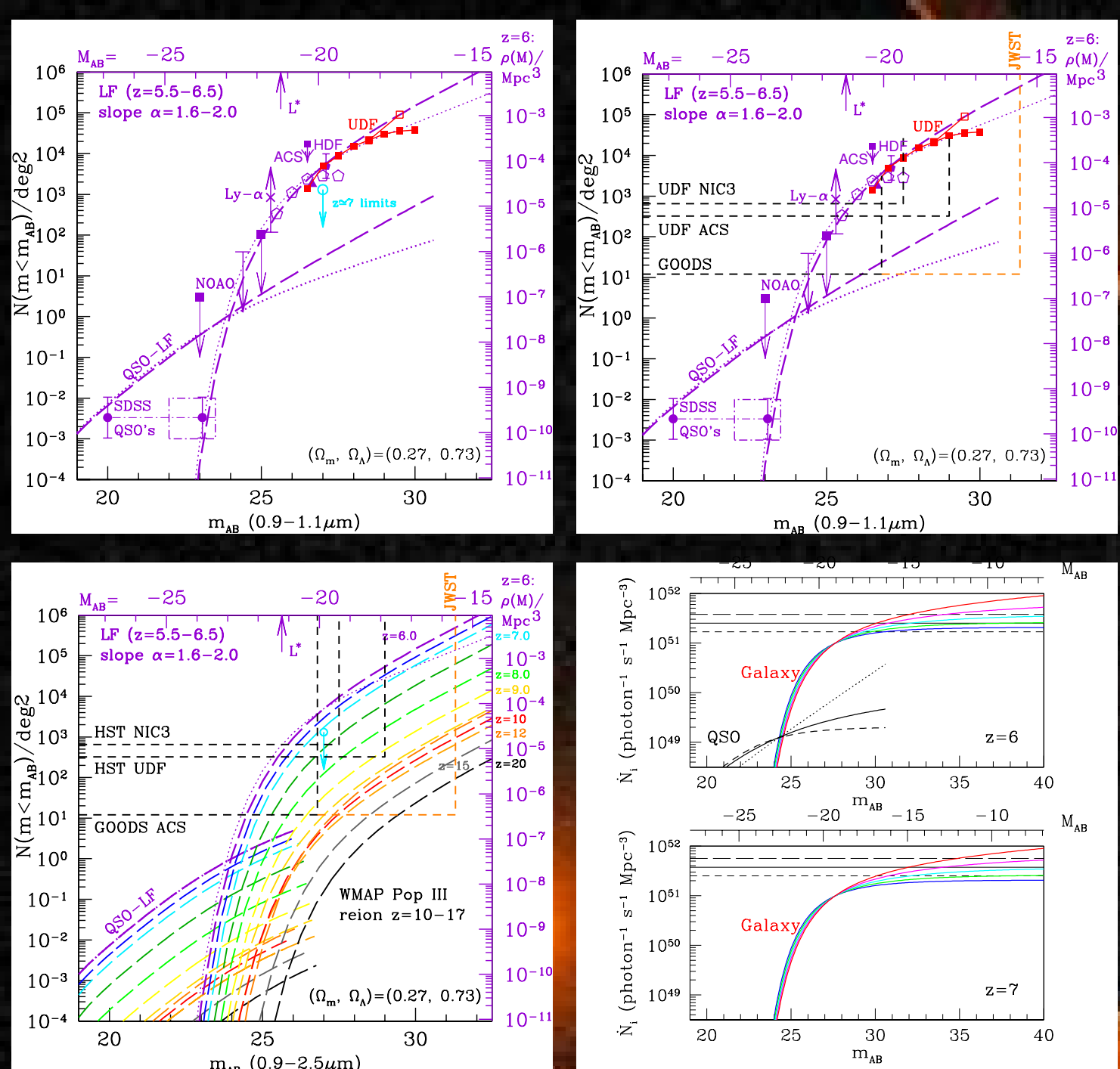
## Outline

- (1) What is JWST and how will it be deployed?  
(see posters 210.01–03 by Clampin et al., Hull et al., and Bowers et al.)
- (2) What instruments and sensitivity will JWST have?  
(see posters 210.04–06 by Rieke et al., Rausscher, and Rieke et al.)
- (3) How can JWST measure First Light and Reionization?
- (4) How can JWST measure Galaxy Assembly
- (5) Predicted Galaxy Appearance for JWST at  $z\sim 1\text{--}15$
- (6) How JWST’s short- $\lambda$  performance affects measurements of faint galaxy parameters
- (7) Will deep JWST images run into the confusion limit?

ASU ALABAMA STATE UNIVERSITY

Sponsored by NASA/JWST

## (3) How JWST will measure First Light and Reionization



[TOP-LEFT] The HUDF showed that the LF of  $z\sim 6$  objects may be very steep, with faint-end and Schechter slope  $\alpha \approx 1.6\text{--}2.0$  (Yan & Windhorst 2004a,b).  
⇒ Dwarf galaxies and not quasars likely completed the reionization epoch at  $z\sim 6$ . This is what JWST will observe in detail to  $z\sim 20$ .

[TOP-RIGHT] HST/ACS has made significant progress at  $z\sim 6$ , surveying very large areas (GOODS, GEMS, COSMOS), or using very long integrations (HUDF). ACS can detect objects at  $z\sim 6.5$ , but its discovery space  $A \times \Omega \times \Delta \log(\lambda)$  cannot map the entire reionization epoch. NICMOS similarly is limited to  $z\sim 8\text{--}10$ .  
⇒ Only JWST will allow us to trace the early reionization epoch.

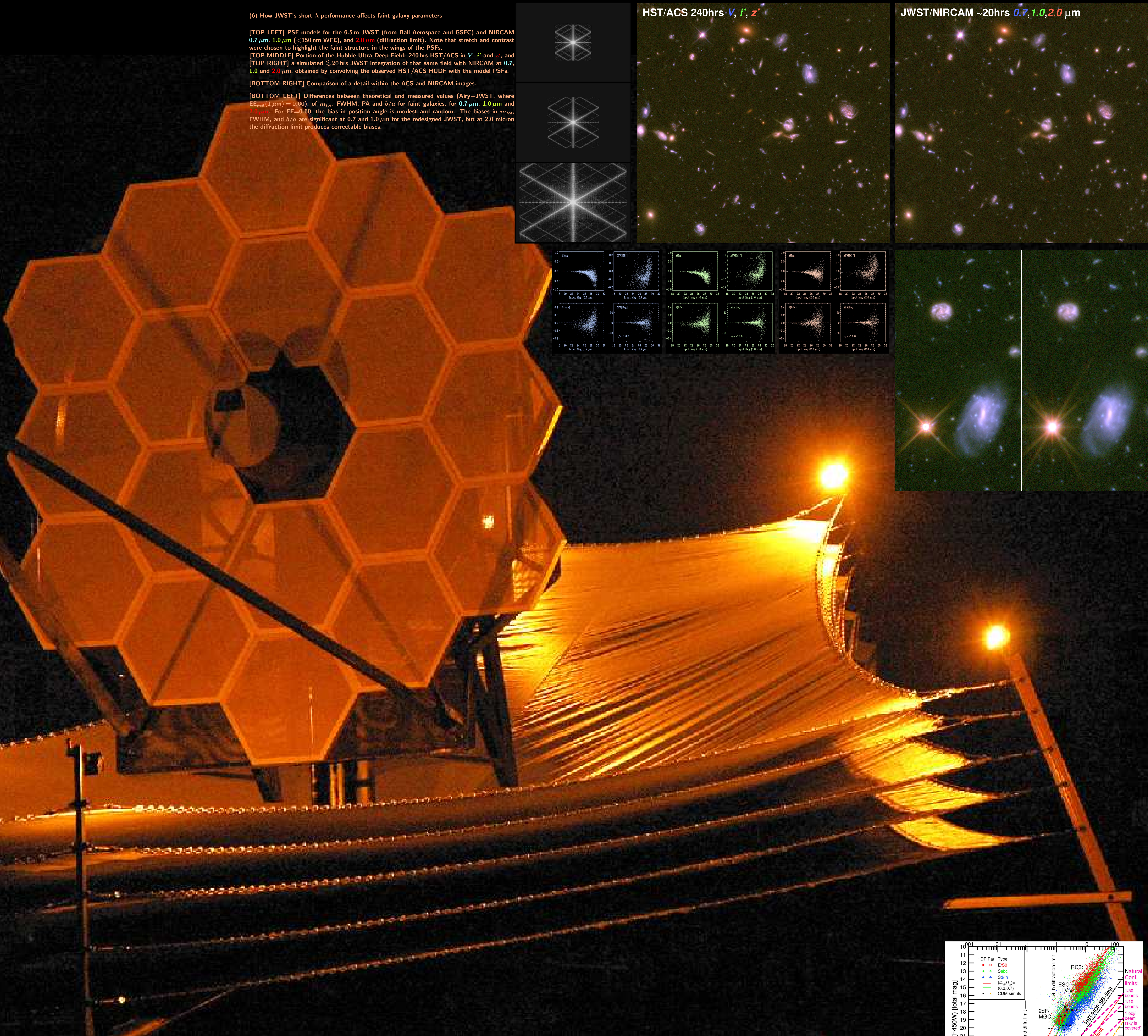
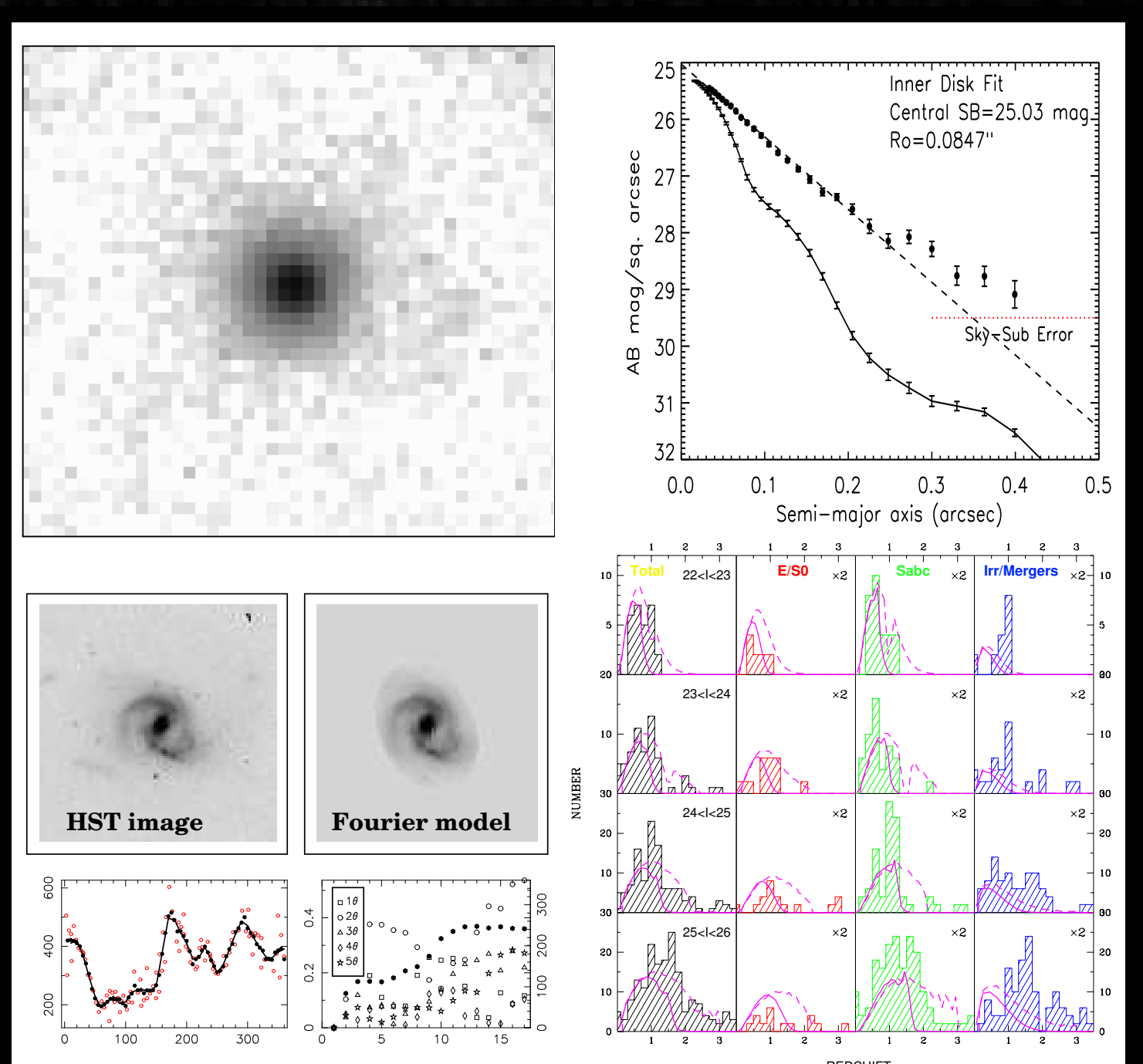
[BOTTOM-LEFT] For JWST to see First Light sources in realistic model scenarios, it needs to have the quoted sensitivity/aperture (A), field-of-view ( $\Omega$ ), and  $\lambda$ -range (0.7–20  $\mu\text{m}$ ) to see Ly-break galaxies and their UV-continuum to  $z\sim 20$ . The JWST design assumes that objects at  $z\sim 20$  are rare, since the volume element is small and JWST samples the brighter part of the LF at  $z\sim 10$ .

[BOTTOM-RIGHT] A steep LF of  $z\sim 6$  objects (Yan & Windhorst 2004) could provide enough UV photons to complete the reionization epoch at  $z\sim 6$ .  
• Pop II dwarf galaxies may not have started shining pervasively much before  $z\sim 7\text{--}8$ , or no HI would be seen in the foreground of  $z\sim 6$  quasars.  
• JWST will measure this ubiquitous population of dwarf galaxies from the end of the reionization epoch at  $z\sim 6$  into the epoch of First Light (Pop III stars) at  $z\sim 10\text{--}20$ .

## (4) How JWST will measure Galaxy Assembly

- Galaxies of all types formed over a wide range of cosmic time, but with a notable transition around  $z\sim 0.5\text{--}1.0$ .
- Sub-galactic units rapidly merge from  $z\sim 7\text{--}1$ , growing into bigger units.
- Merger products start to settle as galaxies with giant bulges and/or large disks around  $z\sim 1$ . These evolved mostly passively since then, resulting in the giant galaxies that we see today.

JWST can measure how galaxies of all types formed over a wide range of cosmic time, by accurately measuring their distribution over rest-frame structure and type as a function of redshift or cosmic epoch. This needs to take the morphological K-correction into account, which is anchored in the UV structure of nearby galaxies (Taylor-Mager et al. 2007 in press; Windhorst et al. 2002).



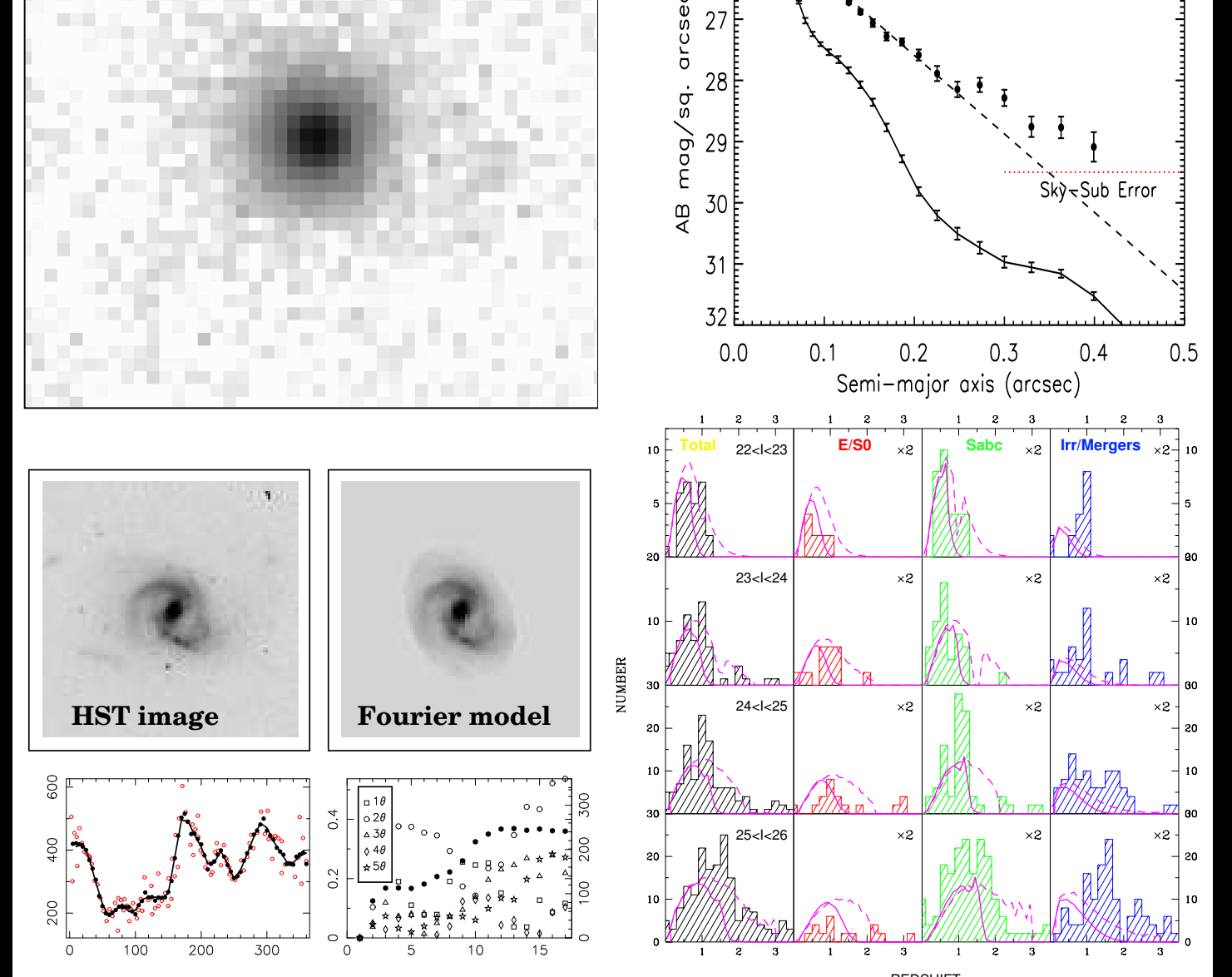
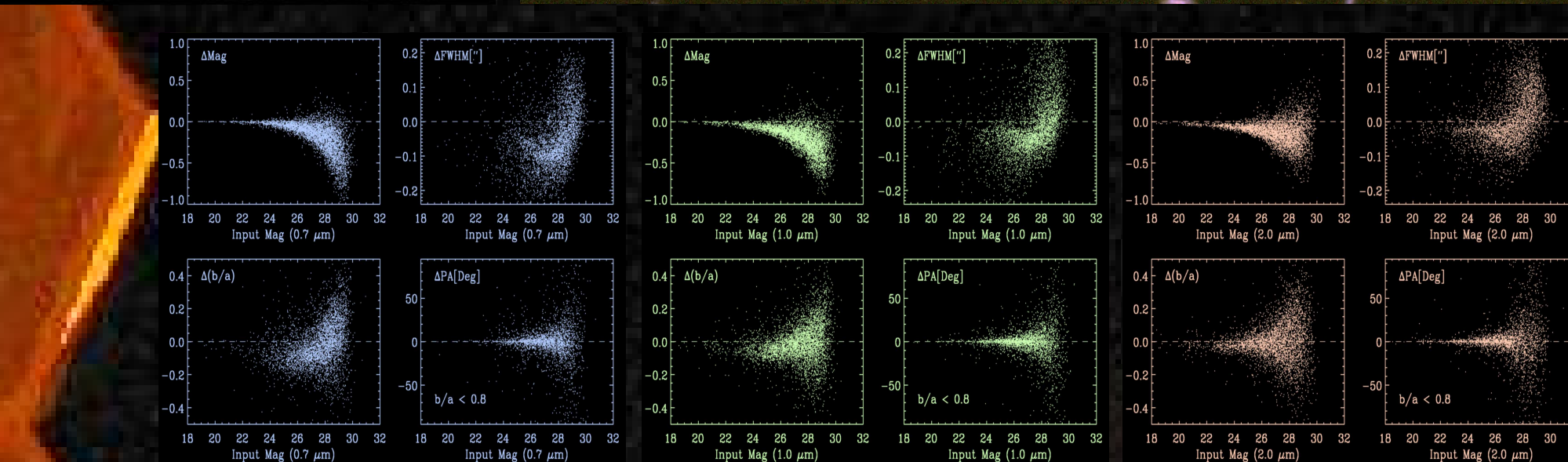
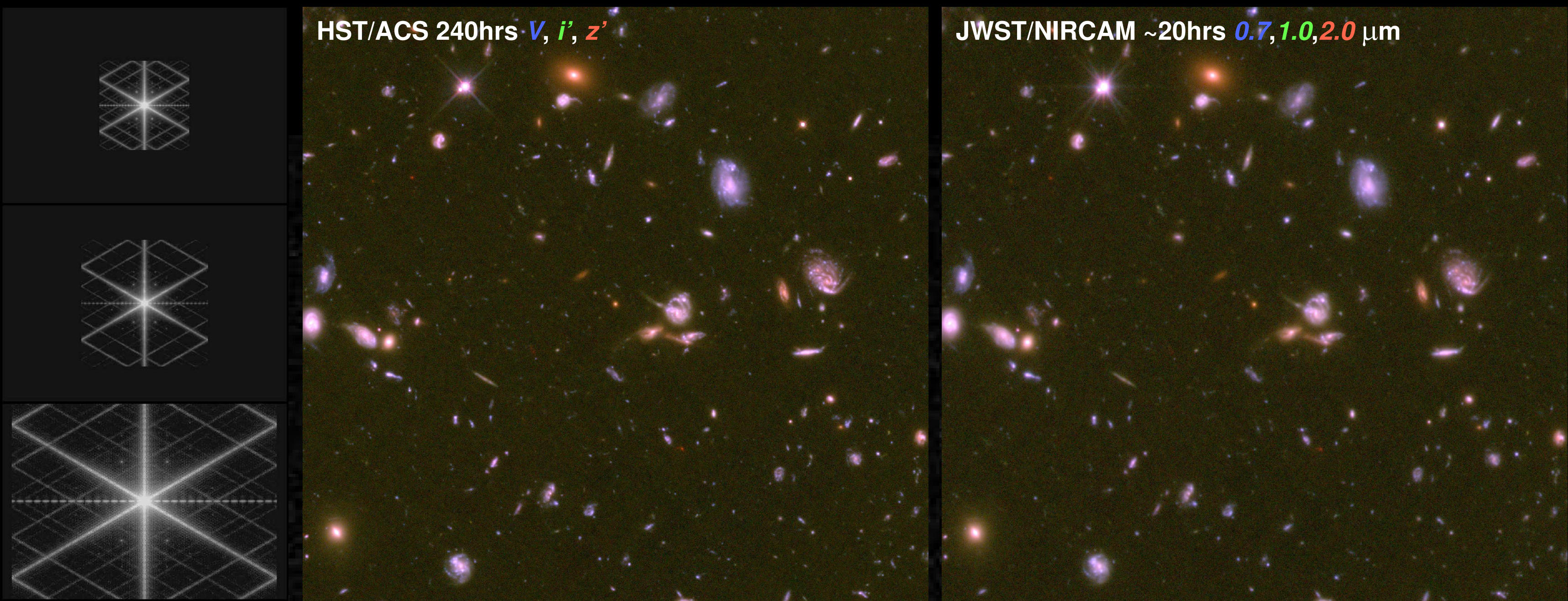
## (6) How JWST’s short- $\lambda$ performance affects faint galaxy parameters

[TOP LEFT] PSF models for the 6.5 m JWST (from Ball Aerospace and GSFC) and NIRCAM 0.7  $\mu\text{m}$ , 1.0  $\mu\text{m}$  ( $<150$  nm WFE), and 2.0  $\mu\text{m}$  (diffraction limit). Note that stretch and contrast were chosen to highlight the faint structure in the wings of the PSFs.

[TOP MIDDLE] Portion of the Hubble Ultra-Deep Field: 240 hrs HST/ACS in V, I, and Z, and [TOP RIGHT] a simulated  $\sim 20$  hrs JWST integration of that same field with NIRCAM at 0.7, 1.0 and 2.0  $\mu\text{m}$ , obtained by convolving the observed HST/ACS HUDF with the model PSFs.

[BOTTOM LEFT] Comparison of a detail within the ACS and NIRCAM images.

[BOTTOM RIGHT] Differences between theoretical and measured values (Airy–JWST, where  $EE_{\text{sim}}(1 \mu\text{m})=0.60$ ), of  $m_{\text{eff}}$ , FWHM, PA and  $b/a$  for faint galaxies, for 0.7  $\mu\text{m}$ , 1.0  $\mu\text{m}$  and 2.0  $\mu\text{m}$ . For  $EE=0.60$ , the bias in position angle is modest and random. The biases in  $m_{\text{eff}}$ , FWHM, and  $b/a$  are significant at 0.7 and 1.0  $\mu\text{m}$  for the redesigned JWST, but at 2.0 micron the diffraction limit produces correctable biases.



(See also poster 171.02 by N. Hathi et al., poster 171.03 by R. Ryan et al., poster 171.04 by A. Straughn et al., and poster 019.01 by S. Cohen et al.)

[FAR LEFT-TOP] Sum of 49 isolated  $z$ -drops:  $\sim 5000$  hrs HUDF in  $z$ -band, which is equivalent to  $\sim 330$  hrs with JWST at 1  $\mu\text{m}$ . [LEFT-TOP] The composite ACS surface brightness profile, PSF and sky-error deviates from that of an exponential disk at  $r_r \gtrsim 0.25''$  ⇒ Dynamical age ( $z \approx 6$ )  $\approx 100\text{--}200$  Myr.

• HST/ACS cannot accurately measure surface brightness profiles of individual  $z \approx 6$  objects, but JWST can do this in detail for  $z \gtrsim 6$  in very long integrations. Dynamical time scales  $\approx$  SED time scale ⇒ Bulk of Pop II SF at  $z_f \approx 7.0 \pm 0.5?$

[FAR LEFT-BOTTOM] Fourier Decomposition is a robust technique of measuring galaxy morphology and structure in a quantitative way (Odehwan et al. 2002).

- Fourier series are fit to the signal in successive concentric annuli
- Even Fourier components describe asymmetric parts (arms, rings, bars)
- Odd Fourier components describe symmetric parts (spurs, lopsided arms, bars, etc.)

JWST can measure the evolution of such features directly.

[LEFT-BOTTOM] JWST can measure how galaxies of all types formed over a wide range of cosmic time, by measuring their redshift distribution as a function of rest-frame type, or as function of a particular Fourier component. (Figure from Driver et al. 1999, ApJ 516, 433).  
• For this, the types must be well imaged for large samples from deep uniform, and high-quality multi-wavelength images — which JWST can do.

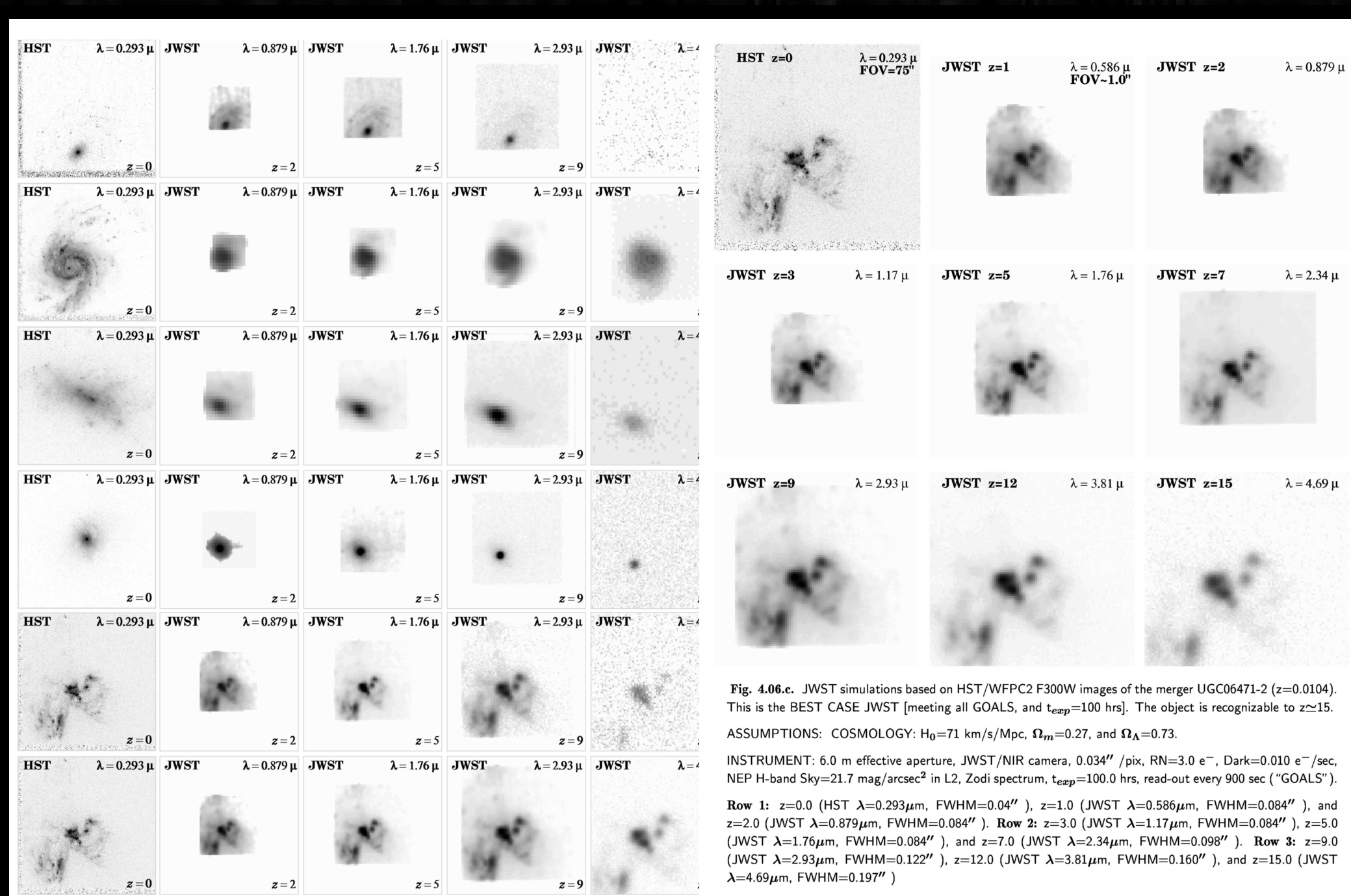


Fig. 486A. JWST simulations based on HST/WFPC2 F300W images of the galaxy UGC02472 (z=0.0204). This is the BEST CASE JWST (meeting all GOALS, and  $t_{\text{exp}}=100$  hr). The object is resolvable to  $z=15$ . ASSUMPTIONS: COSMOS-050;  $\mu_{\text{UV}}=11$ ;  $\mu_{\text{opt}}=16$ ;  $\mu_{\text{IR}}=27$ ; and  $\Omega_{\text{UV}}=0.71$ . Disk=0.03  $''$ ;  $\mu_{\text{UV}}=21.7$  mag/arcsec<sup>2</sup> in L2; 2000 spectrum;  $t_{\text{exp}}=1000$  hrs, readout every 900 sec (‘‘GOALS’’); NIP H-band  $\Delta z=21.7$  mag/arcsec<sup>2</sup> in L2; 2000 spectrum;  $t_{\text{exp}}=1000$  hrs, readout every 900 sec (‘‘GOALS’’). Row 1: z=0.0204 (HST  $\lambda=0.29\mu\text{m}$ , FWHM=0.04 $''$ ), z=0.0204 (JWST  $\lambda=0.50\mu\text{m}$ , FWHM=0.04 $''$ ), and z=0.0204 (JWST  $\lambda=0.70\mu\text{m}$ , FWHM=0.04 $''$ ). Row 2: z=0.0204 (HST  $\lambda=0.29\mu\text{m}$ , FWHM=0.04 $''$ ), z=0.0204 (JWST  $\lambda=0.50\mu\text{m}$ , FWHM=0.04 $''$ ), and z=0.0204 (JWST  $\lambda=0.70\mu\text{m}$ , FWHM=0.04 $''$ ). Row 3: z=0.0204 (HST  $\lambda=0.29\mu\text{m}$ , FWHM=0.04 $''$ ), z=0.0204 (JWST  $\lambda=0.50\mu\text{m}$ , FWHM=0.04 $''$ ), and z=0.0204 (JWST  $\lambda=0.70\mu\text{m}$ , FWHM=0.04 $''$ ). Row 4: z=0.0204 (HST  $\lambda=0.29\mu\text{m}$ , FWHM=0.04 $''$ ), z=0.0204 (JWST  $\lambda=0.50\mu\text{m}$ , FWHM=0.04 $''$ ), and z=0.0204 (JWST  $\lambda=0.70\mu\text{m}$ , FWHM=0.04 $''$ ). Row 5: z=0.0204 (HST  $\lambda=0.29\mu\text{m}$ , FWHM=0.04 $''$ ), z=0.0204 (JWST  $\lambda=0.50\mu\text{m}$ , FWHM=0.04 $''$ ), and z=0.0204 (JWST  $\lambda=0.70\mu\text{m}$ , FWHM=0.04 $''$ ). Row 6: z=0.0204 (HST  $\lambda=0.29\mu\text{m}$ , FWHM=0.04 $''$ ), z=0.0204 (JWST  $\lambda=0.50\mu\text{m}$ , FWHM=0.04 $''$ ), and z=0.0204 (JWST  $\lambda=0.70\mu\text{m}$ , FWHM=0.04 $''$ ). Row 7: z=0.0204 (HST  $\lambda=0.29\mu\text{m}$ , FWHM=0.04 $''$ ), z=0.0204 (JWST  $\lambda=0.50\mu\text{m}$ , FWHM=0.04 $''$ ), and z=0.0204 (JWST  $\lambda=0.70\mu\text{m}$ , FWHM=0.04 $''$ ). Row 8: z=0.0204 (HST  $\lambda=0.29\mu\text{m}$ , FWHM=0.04 $''$ ), z=0.0204 (JWST  $\lambda=0.50\mu\text{m}$ , FWHM=0.04 $''$ ), and z=0.0204 (JWST  $\lambda=0.70\mu\text{m}$ , FWHM=0.04 $''$ ). Row 9: z=0.0204 (HST  $\lambda=0.29\mu\text{m}$ , FWHM=0.04 $''$ ), z=0.0204 (JWST  $\lambda=0.50\mu\text{m}$ , FWHM=0.04 $''$ ), and z=0.0204 (JWST  $\lambda=0.70\mu\text{m}$ , FWHM=0.04 $''$ ). Row 10: z=0.0204 (HST  $\lambda=0.29\mu\text{m}$ , FWHM=0.04 $''$ ), z=0.0204 (JWST  $\lambda=0.50\mu\text{m}$ , FWHM=0.04 $''$ ), and z=0.0204 (JWST  $\lambda=0.70\mu\text{m}$ , FWHM=0.04 $''$ ). Row 11: z=0.0204 (HST  $\lambda=0.29\mu\text{m}$ , FWHM=0.04 $''$ ), z=0.0204 (JWST  $\lambda=0.50\mu\text{m}$ , FWHM=0.04 $''$ ), and z=0.0204 (JWST  $\lambda=0.70\mu\text{m}$ , FWHM=0.04 $''$ ). Row 12: z=0.0204 (HST  $\lambda=0.29\mu\text{m}$ , FWHM=0.04 $''$ ), z=0.0204 (JWST  $\lambda=0.50\mu\text{m}$ , FWHM=0.04 $''$ ), and z=0.0204 (JWST  $\lambda=0.70\mu\text{m}$ , FWHM=0.04 $''$ ). Row 13: z=0.0204 (HST  $\lambda=0.29\mu\text{m}$ , FWHM=0.04 $''$ ), z=0.0204 (JWST  $\lambda=0.50\mu\text{m}$ , FWHM=0.04 $''$ ), and z=0.0204 (JWST  $\lambda=0.70\mu\text{m}$ , FWHM=0.04 $''$ ). Row 14: z=0.0204 (HST  $\lambda=0.29\mu\text{m}$ , FWHM=0.04 $''$ ), z=0.0204 (JWST  $\lambda=0.50\mu\text{m}$ , FWHM=0.04 $''$ ), and z=0.0204 (JWST  $\lambda=0.70\mu\text{m}$ , FWHM=0.04 $''$ ). Row 15: z=0.0204 (HST  $\lambda=0.29\mu\text{m}$ , FWHM=0.04 $''$ ), z=0.0204 (JWST  $\lambda=0.50\mu\text{m}$ , FWHM=0.04 $''$ ), and z=0.0204 (JWST  $\lambda=0.70\mu\text{m}$ , FWHM=0.04 $''$ ). Row 16: z=0.0204 (HST  $\lambda=0.29\mu\text{m}$ , FWHM=0.04 $''$ ), z=0.0204 (JWST  $\lambda=0.50\mu\text{m}$ , FWHM=0.04 $''$ ), and z=0.0204 (JWST  $\lambda=0.70\mu\text{m}$ , FWHM=0.04 $''$ ). Row 17: z=0.0204 (HST  $\lambda=0.29\mu\text{m}$ , FWHM=0.04 $''$ ), z=0.0204 (JWST  $\lambda=0.50\mu\text{m}$ , FWHM=0.04 $''$ ), and z=0.0204 (JWST  $\lambda=0.70\mu\text{m}$ , FWHM=0.04 $''$ ). Row 18: z=0.0204 (HST  $\lambda=0.29\mu\text{m}$ , FWHM=0.04 $''$ ), z=0.0204 (JWST  $\lambda=0.50\mu\text{m}$ , FWHM=0.04 $''$ ), and z=0.0204 (JWST  $\lambda=0.70\mu\text{m}$ , FWHM=0.04 $''$ ). Row 19: z=0.0204 (HST  $\lambda=0.29\mu\text{m}$ , FWHM=0.04 $''$ ), z=0.0204 (JWST  $\lambda=0.50\mu\text{m}$ , FWHM=0.04 $''$ ), and z=0.0204 (JWST  $\lambda=0.70\mu\text{m}$ , FWHM=0.04 $''$ ). Row 20: z=0.0204 (HST  $\lambda=0.29\mu\text{m}$ , FWHM=0.04 $''$ ), z=0.0204 (JWST  $\lambda=0.50\mu\text{m}$ , FWHM=0.04 $''$ ), and z=0.0204 (JWST  $\lambda=0.70\mu\text{m}$ , FWHM=0.04 $''$ ). Row 21: z=0.0204 (HST  $\lambda=0.29\mu\text{m}$ , FWHM=0.04 $''$ ), z=0.0204 (JWST  $\lambda=0.50\mu\text{m}$ , FWHM=0.04 $''$ ), and z=0.0204 (JWST  $\lambda=0.70\mu\text{m}$ , FWHM=0.04 $''$ ). Row 22: z=0.0204 (HST  $\lambda=0.29\mu\text{m}$ , FWHM=0.04 $''$ ), z=0.0204 (JWST  $\lambda=0.50\mu\text{m}$ , FWHM=0.04 $''$ ), and z=0.0204 (JWST  $\lambda=0.70\mu\text{m}$ , FWHM=0.04 $''$ ). Row 23: z=0.0204 (HST  $\lambda=0.29\mu\text{m}$ , FWHM=0.04 $''$ ), z=0.0204 (JWST  $\lambda=0.50\mu\text{m}$ , FWHM=0.04 $''$ ), and z=0.0204 (JWST  $\lambda=0.70\mu\text{m}$ , FWHM=0.04 $''$ ). Row 24: z=0.0204 (HST  $\lambda=0.29\mu\text{m}$ , FWHM=0.04 $''$ ), z=0.0204 (JWST  $\lambda=0.50\mu\text{m}$ , FWHM=0.04 $''$ ), and z=0.0204 (JWST  $\lambda=0.70\mu\text{m}$ , FWHM=0.04 $''$ ). Row 25: z=0.0204 (HST  $\lambda=0.29\mu\text{m}$ , FWHM=0.04 $''$ ), z=0.0204 (JWST  $\lambda=0.50\mu\text{m}$ , FWHM=0.04 $''$ ), and z=0.0204 (JWST  $\lambda=0.70\mu\text{m}$ , FWHM=0.04 $''$ ). Row 26: z=0.0204 (HST  $\lambda=0.29\mu\text{m}$ , FWHM=0.04 $''$ ), z=0.0204 (JWST  $\lambda=0.50\mu\text{m}$ , FWHM=0.04 $''$ ), and z=0.0204 (JWST  $\lambda=0.70\mu\text{m}$ , FWHM=0.04 $''$ ). Row 27: z=0.0204 (HST  $\lambda=0.29\mu\text{m}$ , FWHM=0.04 $''$ ), z=0.0204 (JWST  $\lambda=0.50\mu\text{m}$ , FWHM=0.04 $''$ ), and z=0.0204 (JWST  $\lambda=0.70\mu\text{m}$ , FWHM=0.04 $''$ ). Row 28: z=0.0204 (HST  $\lambda=0.29\mu\text{m}$ , FWHM=0.04 $''$ ), z=0.0204 (JWST  $\lambda=0.50\mu\text{m}$ , FWHM=0.04 $''$ ), and z=0.0204 (JWST  $\lambda=0.70\mu\text{m}$ , FWHM=0.04 $''$ ). Row 29: z=0.0204 (HST  $\lambda=0.29\mu\text{m}$ , FWHM=0.04 $''$ ), z=0.0204 (JWST  $\lambda=0.50\mu\text{m}$ , FWHM=0.04 $''$ ), and z=0.0204 (JWST  $\lambda=0.70\mu\text{m}$ , FWHM=0.04 $''$ ). Row 30: z=0.0204 (HST  $\lambda=0.29\mu\text{m}$ , FWHM=0.04 $''$ ), z=0.0204 (JWST  $\lambda=0.50\mu\text{m}$ , FWHM=0.04 $''$ ), and z=0.0204 (JWST  $\lambda=0.70\mu\text{m}$ , FWHM=0.04 $''$ ). Row 31: z=0.0204 (HST  $\lambda=0.29\mu\text{m}$ , FWHM=0.04 $''$ ), z=0.0204 (JWST  $\lambda=0.50\mu\text{m}$ , FWHM=0.04 $''$ ), and z=0.0204 (JWST  $\lambda=0.70\mu\text{m}$ , FWHM=0.04 $''$ ). Row 32: z=0.0204 (HST  $\lambda=0.29\mu\text{m}$ , FWHM=0.04 $''$ ), z=0.0204 (JWST  $\lambda=0.50\mu\text{m}$ , FWHM=0.04 $''$ ), and z=0.0204 (JWST  $\lambda=0.70\mu\text{m}$ , FWHM=0.04 $''$ ). Row 33: z=0.0204 (HST  $\lambda=0.29\mu\text{m}$ , FWHM=0.04 $''$ ), z=0.0204 (JWST  $\lambda=0.50\mu\text{m}$ , FWHM=0.04 $''$ ), and z=0.0204 (JWST  $\lambda=0.70\mu\text{m}$ , FWHM=0.04 $''$ ). Row 34: z=0.0204 (HST  $\lambda=0.29\mu\text{m}$ , FWHM=0.04 $''$ ), z=0.0204 (JWST  $\lambda=0.50\mu\text{m}$ , FWHM=0.04 $''$ ), and z=0.0204 (JWST  $\lambda=0.70\mu\text{m}$ , FWHM=0.04 $''$ ). Row 35: z=0.0204 (HST  $\lambda=0.29\mu\text{m}$ , FWHM=0.04 $''$ ), z=0.0204 (JWST  $\lambda=0.50\mu\text{m}$ , FWHM=0.04 $''$ ), and z=0.0204 (JWST  $\lambda=0.70\mu\text{m}$ , FWHM=0.04 $''$ ). Row 36: z=0.0204 (HST  $\lambda=0.29\mu\text{m}$ , FWHM=0.04 $''$ ), z=0.0204 (JWST  $\lambda=0.50\mu\text{m}$ , FWHM=0.04 $''$ ), and z=0.0204 (JWST  $\lambda=0.70\mu\text{m}$ , FWHM=0.04 $''$ ). Row 37: z=0.0204 (HST  $\lambda=0.29\mu\text{m}$ , FWHM=0.04 $''$ ), z=0.0204 (JWST  $\lambda=0.50\mu\text{m}$ , FWHM=0.04 $''$ ), and z=0.0204 (JWST  $\lambda=0.70\mu\text{m}$ , FWHM=0.04 $''$ ). Row 38: z=0.0204 (HST  $\lambda=0.29\mu\text{m}$ , FWHM=0.04 $''$ ), z=0.0204 (JWST  $\lambda=0.50\mu\text{m}$ , FWHM=0.04 $''$ ), and z=0.0204 (JWST  $\lambda=0.70\mu\text{m}$ , FWHM=0.04 $''$ ). Row 39: z=0.0204 (HST  $\lambda=0.29\mu\text{m}$ , FWHM=0.04 $''$ ), z=0.0204 (JWST  $\lambda=0.50\mu\text{m}$ , FWHM=0.04 $''$ ), and z=0.0204 (JWST  $\lambda=0.70\mu\text{m}$ , FWHM=0.04 $''$ ). Row 40: z=0.0204 (HST  $\lambda=0.29\mu\text{m}$ , FWHM=0.04 $''$ ), z=0.0204 (JWST  $\lambda=0.50\mu\text{m}$ , FWHM=0.04 $''$ ), and z=0.0204 (JWST  $\lambda=0.70\mu\text{m}$ , FWHM=0.04 $''$ ). Row 41: z=0.0204 (HST  $\lambda=0.29\mu\text{m}$ , FWHM=0.04 $''$ ), z=0.0204 (JWST  $\lambda=0.50\mu\text{m}$ , FWHM=0.04 $''$ ), and z=0.0204 (JWST  $\lambda=0.70\mu\text{m}$ , FWHM=0.04 $''$ ). Row 42: z=0.0204 (HST  $\lambda=0.29\mu\text{m}$ , FWHM=0.04 $''$ ), z=0.0204 (JWST  $\lambda=0.50\mu\text{m}$ , FWHM=0.04 $''$ ), and z=0.0204 (JWST  $\lambda=0.70\mu\text{m}$ , FWHM=0.04 $''$ ). Row 43: z=0.0204 (HST  $\lambda=0.29\mu\text{m}$ , FWHM=0.04 $''$ ), z=0.0204 (JWST  $\lambda=0.50\mu\text{m}$ , FWHM=0.04 $''$ ), and z=0.0204 (JWST  $\lambda=0.70\mu\text{m}$ , FWHM=0.04 $''$ ). Row 44: z=0.0204 (HST  $\lambda=0.29\mu\text{m}$ , FWHM=0.04 $''$ ), z=0.0204 (JWST  $\lambda=0.50\mu\text{m}$ , FWHM=0.04 $''$ ), and z=0.0204 (JWST  $\lambda=0.70\mu\text{m}$ , FWHM=0.04 $''$ ). Row 45: z=0.0204 (HST  $\lambda=0.29\mu\text{m}$ , FWHM=0.04 $''$ ), z=0.0204 (JWST  $\lambda=0.50\mu\text{m}$ , FWHM=0.04 $''$ ), and z=0.0204 (JWST  $\lambda=0.70\mu\text{m}$ , FWHM=0.04 $''$ ). Row 46: z=0.0204 (HST  $\lambda=0.29\mu\text{m}$ , FWHM=0.04 $''$ ), z=0.0204 (JWST  $\lambda=0.50\mu\text{m}$ , FWHM=0.04 $''$ ), and z=0.0204 (JWST  $\lambda=0.70\mu\text{m}$ , FWHM=0.04 $''$ ). Row 47: z=0.0204 (HST  $\lambda=0.29\mu\text{m}$ , FWHM=0.04 $''$ ), z=0.0204 (JWST  $\lambda=0.50\mu\text{m}$ , FWHM=0.04 $''$ ), and z=0.0204 (JWST  $\lambda=0.70\mu\text{m}$ , FWHM=0.04 $''$ ). Row 48: z=0.0204 (HST  $\lambda=0.29\mu\text{m}$ , FWHM=0.04 $''$ ), z=0.0204 (JWST  $\lambda=0.50\mu\text{m}$ , FWHM=0.04 $''$ ), and z=0.0204 (JWST  $\lambda=0.70\mu\text{m}$ , FWHM=0.04 $''$ ). Row 49: z=0.0204 (HST  $\lambda=0.29\mu\text{m}$ , FWHM=0.04 $''$ ), z=0.0204 (JWST  $\lambda=0.50\mu\text{m}$ , FWHM=0.04 $''$ ), and z=0.0204 (JWST  $\lambda=0.70\mu\text{m}$ , FWHM=0.04 $''$ ). Row 50: z=0.0204 (HST  $\lambda=0.29\mu\text{m}$ , FWHM=0.04 $''$ ), z=0.0204 (JWST  $\lambda=0.50\mu\text{m}$ , FWHM=0.04 $''$ ), and z=0.0204 (JWST  $\lambda=0.70\mu\text{m}$ , FWHM=0.04 $''$ ). Row 51: z=0.0204 (HST  $\lambda=0.29\mu\text{m}$ , FWHM=0.04 $''$ ), z=0.0204 (JWST  $\lambda=0.50\mu\text{m}$ , FWHM=0.04 $''$ ), and z=0.0204 (JWST  $\lambda=0.70\mu\text{m}$ , FWHM=0.04 $''$ ). Row 52: z=0.0204 (HST  $\lambda=0.29\mu\text{m}$ , FWHM=0.04 $''$ ), z=0.0204 (JWST  $\lambda=0.50\mu\text{m}$ , FWHM=0.04 $''$ ), and z=0.0204 (JWST  $\lambda=0.70\mu\text{m}$ , FWHM=0.04 $''$ ). Row 53: z=0.0204 (HST  $\lambda=0.29\mu\text{m}$ , FWHM=0.04 $''$ ), z=0.0204 (JWST  $\lambda=0.50\mu\text{m}$ , FWHM=0.04 $''$ ), and z=0.0204 (JWST  $\lambda=0.70\mu\text{m}$ , FWHM=0.04 $''$ ). Row 54: z=0.0204 (HST  $\lambda=0.29\mu\text{m}$ , FWHM=0.04 $''$ ), z=0.0204 (JWST  $\lambda=0.50\mu\text{m}$ , FWHM=0.04 $''$ ), and z=0.0204 (JWST  $\lambda=0.70\mu\text{m}$ , FWHM=0.04 $''$ ). Row 55: z=0.0204 (HST  $\lambda=0.29\mu\text{m}$ , FWHM=0.04 $''$ ), z=0.0204 (JWST  $\lambda=0.50\mu\text$